

# Observing the Inverse melting of the vortex lattice in $\text{Bi}_2\text{Sr}_2\text{CaCu}_2\text{O}_8$ with point defects using Langevin simulations with vortex shaking

Yadin Y. Goldschmidt and Jin-Tao Liu

*Department of Physics and Astronomy, University of Pittsburgh, Pittsburgh, Pennsylvania 15260*

(Dated: October 9, 2018)

Langevin dynamics simulations of the vortex matter in the highly-anisotropic high-temperature superconductor  $\text{Bi}_2\text{Sr}_2\text{CaCu}_2\text{O}_8$  were performed. We introduced point defects as a smoothed distribution of a random potential. Both the electromagnetic and Josephson interactions among pancake vortices were included. A special shaking and annealing process was introduced to let the system approach the equilibrium configuration. We are able to see the inverse melting transition from the Bragg-glass to the amorphous vortex glass state, in agreement with recent experiments.

PACS numbers: 74.25.Dw, 74.25.Qt, 64.70.Q-, 74.72.Hs

Recent experiments have revealed rich and interesting phase diagram of the vortex matter in the anisotropic high-temperature superconductor  $\text{Bi}_2\text{Sr}_2\text{CaCu}_2\text{O}_8$  (BSCCO) when point impurities are present [1, 2, 3, 4, 5, 6]. Point defects are present even in pristine crystalline samples due to oxygen vacancies. In addition, one can increase the concentration of such defects by bombarding the sample with electrons, the energy of which is of the order of a few MeV [2].

In this letter we concentrate on the effect of point disorder on the location and nature of the first order (FO) melting line of the vortex lattice with quasi long-range order into a vortex liquid or an amorphous vortex glass, depending on the temperature. At high temperatures, in the range of  $T \gtrsim 0.5T_c$ , where  $T_c \approx 90\text{K}$  for BSCCO, point defects have only a mild effect on the position of the melting line in the  $T$ - $B$  plane. They shift the melting line of the vortex solid into a disordered vortex liquid to a slightly lower temperature for a given magnetic field [2, 8, 9]. The shift becomes larger as the temperature decreases along the melting line in the  $T$ - $B$  plane until a special point is reached with  $T = T_{sp}$ . Below this temperature the role of the point disorder becomes much more significant and the glassy behavior becomes dominant. For  $T < T_{sp}$  it is expected that the melting transition is from a dislocation free Bragg glass (BrG) into a dislocation rich amorphous vortex glass (VG) phase which replaces the vortex liquid phase (VL) at high fields. The melting line ceases to be a monotonically decreasing function of  $T$  in the  $T$ - $B$  plane, and at least near and below  $T_{sp}$  it is a monotonically increasing function of temperature [5, 6]. Thus as the temperature is lowered for magnetic fields slightly below  $B_{sp}$ , the field corresponding to  $T_{sp}$ , one expects to see first a transition from a VL to a BrG, which is a solid with quasi-long range order [7], and then a second transition into a disordered VG phase. The latter transition, which is quite a rare phenomenon in physical systems, since usually lowering the temperature results in more order, is referred to as the inverse melting transition [4] or sometimes as reentrant behavior [8]. Previous theoretical work on the effects of point

defects on the phase diagram of BSCCO is given in Refs. [7, 8, 9, 10, 11], and previous numerical investigations is given in Refs. [12, 13, 14, 15, 16, 17].

In this work we observed the inverse melting in numerical simulations and obtained a phase diagram in qualitative agreement with experiments. We also investigate the properties of the different phases near the transition, both static and dynamical, and characterize their differences. The method we use for our simulations is Langevin dynamics, also commonly referred to as Brownian dynamics. In BSCCO the flux-lines (FLs) which are threads of magnetic field penetrating the sample and surrounded by revolving currents (vortices) are more faithfully described by stacks of pancake vortices [18], each moving in one  $\text{CuO}_2$  plane, and interacting with each other by electromagnetic interaction as well as by the Josephson interaction. When simulating the dynamics we use the so called over-damped limit where the mass of the pancakes is negligible and the velocity of each pancake is proportional to the force acting on it. This force results from the interaction with other pancakes, from the effect of the defects, from the thermal white noise, and possibly from an applied force typically resulting from a Lorentz force when a global current passes through the sample.

Some of the advantages of using Langevin simulations are that one can control all the interactions precisely, and one can take microscopic pictures and measure physical quantities that are difficult to measure in experiments, like the magnitude of the transverse fluctuations of FLs or the amount of their entanglement. In addition it is possible to measure dynamical properties relating to the pinning and the critical current. It is possible to characterize the differences between the various thermodynamic phases of the vortex matter and check in a controlled way how they result from the applied ingredients and parameters of the model. A main disadvantage of the simulations is that the system simulated is small and hence phase transitions are always broadened and are not as sharp as those observed in real experiments. In our current simulations we use 1296 pancake vortices, 36 in each of 36 planes. The system is a box of size

$6a_0 \times 3\sqrt{3}a_0 \times 36d$  where  $d$  is the  $\text{CuO}_2$  plane separation,  $a_0 = (2\phi_0/\sqrt{3}B)^{1/2}$ ,  $B$  is the magnetic field induction and  $\phi_0$  is the flux quantum. Pairwise interactions among all pancakes are implemented as discussed in detail in Ref. 19, 20, 21. Both electromagnetic and Josephson interactions are included. The former between any pair of pancakes, the latter only between nearest neighbor pancakes belonging to the same stack. Periodic boundary conditions are used in all directions, including  $z$ -direction. We also implement flux cutting and recombination. The critical temperature for BSCCO was assumed to be  $T_c = 90$  K. Other parameters used were  $\lambda(0) = 1700$  Å (penetration depth),  $\xi(0) = 30$  Å (coherence length),  $d = 15$  Å,  $\gamma = 375$  (anisotropy). We assumed that  $\lambda$  and  $\xi$  have temperature dependence that is proportional to  $(1 - T/T_c)^{-1/2}$ .

We now describe in more detail the implementation of the distribution of point defects through the sample. Following Blatter *et al.* [22], we generate a random pinning energy distribution per pancake given by

$$U^p(\vec{u}, z) = d \int \int d^2R U_{pin}(\vec{R}, z) p(\vec{R} - \vec{u}),$$

$$p(\vec{R}) = 2\xi^2 / (R^2 + 2\xi^2), \quad (1)$$

$$\langle U_{pin}(\vec{R}, z) U_{pin}(\vec{R}', z') \rangle = \gamma_U \delta^{(2)}(\vec{R} - \vec{R}') \delta(z - z').$$

Here  $\gamma_U$  gives the variance of the gaussian distributed random variable  $U_{pin}$ .  $\vec{R}$  and  $\vec{u}$  are two dimensional vectors in the layer labeled by  $z$ . Because of the convolution of the uncorrelated random variable with the single pin form factor  $p(\vec{R})$  we obtain a distribution of random numbers with a power law correlation in each layer, uncorrelated among different layers. The equations above are discretized on a fine grid and the integrals are implemented as summations. Typically we used a grid size of  $3a_0/800$ . The value of  $\gamma_U$  used in most of our simulations is  $\gamma_U(T) = \gamma_U(0)(1 - T/T_c)^2$ , with  $\gamma_U(0) = 1.72 \times 10^{-9} \text{erg}^2 \text{cm}^{-3} = 0.09 (\text{k}_B \text{K})^2 \text{Å}^{-3}$ .

We now discuss the results of the simulations. In Fig.1 we show the phase diagram of the system with point disorder using our technique of simulated annealing and vortex shaking. For comparison we show the melting line of the same system without shaking and starting from an ordered configuration of FLs for each temperature and field. Only when using annealing and shaking we are able to see the inverse melting for fields in the range  $350 < B < 450$  G. The BrG phase, VG phase and VL phase are indicated on the figure. Recent experiments also show more subtle second order (SO) transitions between the VG and VL phases and between the BrG and Solid phases. In the present simulations we did not explore these SO transitions, but we indicated their approximate location on the figure as a dotted line as expected from the experimental results. Here we only measure the FO transition line. Actually the order of the transition can only be resolved in the simulation to be of first order

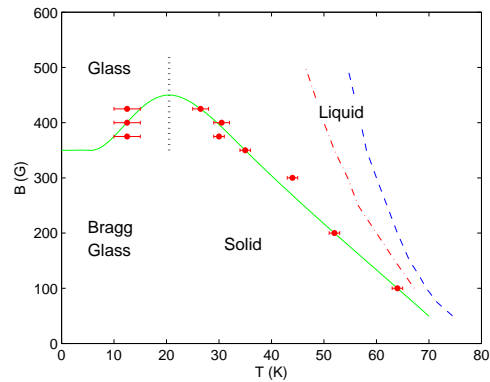


FIG. 1: (color online) Phase diagram. The transition temperatures for vortices with point disorder at various fields were obtained from simulations with simulated annealing and vortex shaking (•, red), and a smooth line (green) is drawn to fit the data. The melting transition of the pure system (dashed, blue) is plotted for comparison, as well as the transition line of the system with point disorder without annealing and shaking (dashed-dot, red).

for small fields  $B < 300$  G by observing a small step in the total energy. For higher fields, since the system is small we cannot resolve the difference between a weak first order and a second order transition.

Next, we give the details of the simulated annealing and vortex shaking procedure. For a given magnetic field, the system is first simulated at a temperature above the melting transition for 180 time units (time is measured [19, 21] in units of  $\eta a_0^2 / \epsilon_0(T)$  where  $\eta$  is the viscous drag coefficient per unit length and  $\epsilon_0(T) = (\phi_0 / 4\pi\lambda(T))^2$ ). We then decrease the temperature by steps of 0.5 K and start each subsequent simulation from the last configuration of the previous run. For each step the simulation time of 180 units is divided as follows: During time intervals 0-40, 80-90 and 130-140 vortex shaking is applied as will be discussed below. After each period of shaking 20 units of time is spent for equilibration and then 20 units of time for measurements. The vortex shaking is implemented by applying alternating forces on all pancakes in adjacent layers. Within the same layer the force is the same on all pancakes then in the next layer it is opposite, and since we have an even number of layers the total force is zero. In addition the shaking force is varying with time as follows: For 0.5 units of time the force is in the  $+x$  direction, in the next 0.5 units of time it is in the  $-x$  direction, and then similarly in the  $\pm y$  direction. This complete a shaking cycle of 2 time units that can be repeated. The strength of the shaking force was taken to be  $F_{shake} = \sqrt{\pi d \gamma_U / 2}$ . Thus it is proportional to the average pinning force. The annealing and shaking procedure helps the system to reach a configuration closer to true thermodynamic equilibrium and prevents it to be stuck in a metastable state.

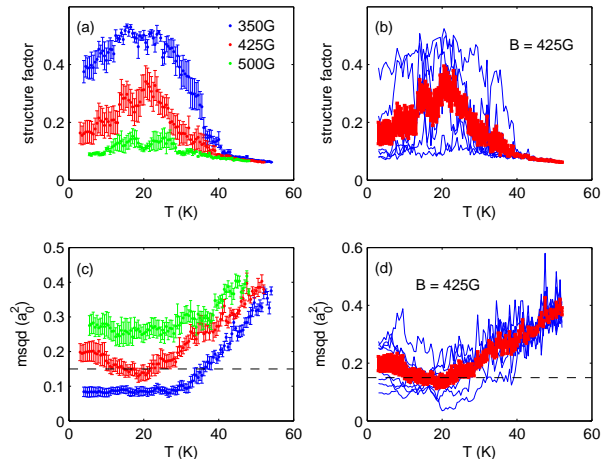


FIG. 2: (color online) Structure factor (SF) and mean square deviation (msqd). (a) SF at 350 G (top, blue), 425 G (middle, red), and 500 G (bottom, green), average over 8 realizations. (b) SF at 425 G (thick red line, average over 8 disorder realizations), the results for each individual realization are shown in the background (thin blue lines). (c) msqd at 350 G (bottom, blue), 425 G (middle red), and 500 G (top, green), average over 8 realizations. (d) msqd at 425 G, similar to (b).

Next we discuss the results of the measurements of the structure factor and the mean square deviation of the FLs. These measurements are depicted in Fig. 2. In Fig. 2(a) we show the normalized structure factor as a function of temperature for three different fields. The structure factor is calculated at the first Bragg peak and is normalized to 1 for perfect crystalline order. This figure shows the average results for 8 different realizations of the random potential. In Figure 2(b) we show the individual realizations for one field (425G) that make up the average. We see that for the lower fields, as the temperature is decreased, the structure factor starts to rise below 40 K and reaches a maximum at about 20 K and then decreases again. If we set the threshold at about 0.2-0.25 then we can say that for  $B = 425\text{G}$  there is a freezing transition at about  $T = 30\text{ K}$  and an inverse melting transition at about  $T = 10\text{ K}$ . For  $B = 350\text{G}$  there is only a freezing transition at about  $T = 35\text{ K}$  and no reentrant behavior. For  $B = 500\text{G}$  there is no transition at all.

In Fig. 2(c) we see the averaged mean square deviation of the FLs from straight lines. In fig. 2(d) we see the eight realizations that make up the average for  $B = 425\text{G}$ . If we take the value of 0.15 as the borderline case we see again that for  $B = 350$  there is a melting transition at around  $T=35\text{ K}$ , for  $B = 425\text{ G}$  there is both a freezing and an inverse melting and for  $B = 500\text{ K}$  there is no transition at all. Figures 2(c) and 2(d) obtained from our actual simulations are very similar to results obtained by Ertas and Nelson [8] (see Figures 3 and 4

in that reference) using the cage model together with a transfer matrix computation of the root mean square deviation. The corresponding  $T^*$  in our case is about 10 K. The reason that the mean square deviation first decreases as one raises the temperature from zero is that thermal fluctuations will initially act to blur the pinning sites and prevent the pancakes to best accommodate the random potential. Thus the pinning energy will be less negative and the Josephson energy will decrease as the FLs become straighter. As the temperature further increases it will make the FLs wiggle more because of thermal motion and the mean square deviation increases.

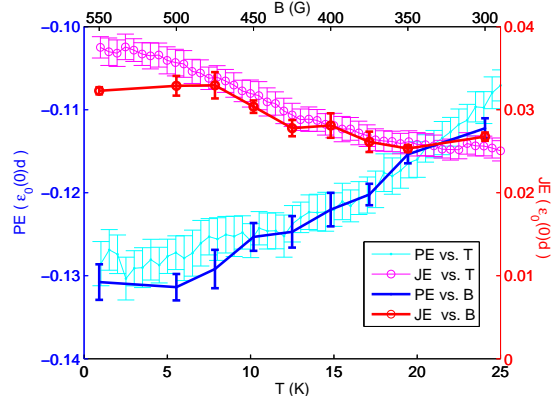


FIG. 3: (color online) Pinning energy (PE) and Josephson energy (JE). The PE (thin, cyan) and JE (thin, magenta) versus  $T$  curves were simulations with  $B = 400\text{ G}$ . The PE (thick, blue) and JE (thick, red) versus  $B$  curves correspond to  $T = 15\text{ K}$ .

This argument can be further supported by observing the pinning and Josephson energies at low temperatures, the latter reflecting the deviation of the FLs from straight stacks. In Fig. 3 we observe the behavior of the pinning energy and Josephson energy as the temperature increase for a fixed field of 400 G. Superimposed are the same energies as a function of decreasing field at fixed temperature of 15 K. In both cases the system changes from the VL phase into the BrG phase. We see the decrease of the effective pinning (pinning energy becomes less negative, so it rises) and this is compensated by a decrease of the Josephson energy, i.e. the FLs become straighter. This is a disorder driven transition so the pinning energy plays a similar role to the entropy in a temperature driven transition, but here the more ordered phase occurs at higher temperature or lower magnetic field as is evident from Fig. 1. For temperatures above 25K the Josephson energy starts to increase again due to increased thermal fluctuations. Fig. 3 shows that decreasing the field at fixed temperature makes the pinning less effective and helps increase the amount of order in the system similarly to increasing the temperature.

To probe further the difference between the BrG and VG phases we measured the fraction of topological de-

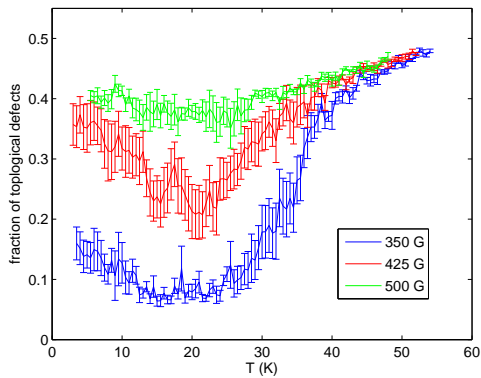


FIG. 4: (color online) Fraction of topological defects. Three different fields are shown: 350 G (bottom, blue), 425 G (middle, red), and 500 G (top, green). The curve for each field is averaged over 8 disorder realizations.

fects (TD). For a given configuration of pancakes we use Delaunay triangulation to measure the number of nearest neighbors for each lattice point. Every deviation from 6 is a topological defect. The fraction of sites with TDs to the total number of sites, averaged over many configurations is depicted in Fig. 4. We see this fraction for three different fields as a function of temperature. If we impose a borderline value of 0.3 we see that for  $B = 350$  G the transition to BrG at 35 K is associated with a decrease in the number of TDs. For  $B = 425$  G there is an inverse melting from BrG to VL which is associated with an increase in the number of TDs. For  $B = 500$  G the fraction of TDs never falls significantly. The abundance of TDs is also present in the liquid so it does not distinguish the VG from a liquid. We can think of the VG as kind of a frozen liquid where the pancakes' positions are frozen near strong pinning sites. We also verified the amount of entanglement is large in the VG similar to the liquid by measuring the number of non-simple loops in the system. Experimentally the transition from BrG to the VG was historically referred to as the “second peak”. As the magnetic field is increased at fixed temperature below  $T_{sp}$ , there is a jump in the critical current at the transition. This jump is associated with an increase in the effective pinning of the FLs, thus making them harder to detach from their equilibrium positions by the applied Lorentz force due to the current. We carried out measurements of the response of the pancakes to an applied force in the  $x$ -direction (related to the I-V characteristics). The results are depicted in Fig. 5 for different fields at  $T = 15$  K. We see that for  $B = 300 - 400$  G the pancakes mobility decreases with increasing field as measured by their velocity under the influence of an applied force. For  $B = 450 - 500$  G there is no longer much change with increasing field and the pinning seems to saturate. This seems consistent with a transition into the VG phase.

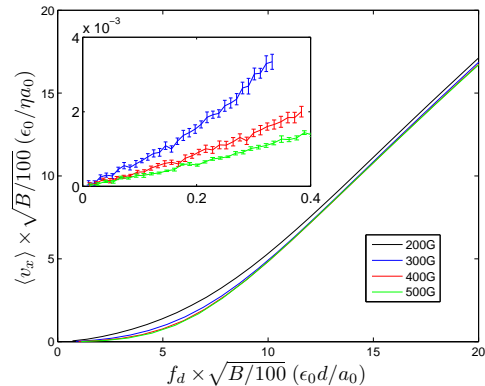


FIG. 5: (color online) Drifting velocity versus driving force at 15K. The results for each field are averages over 8 realizations. For the axes units are chosen such that  $a_0 = a_0(100G)$ ,  $\epsilon_0 = \epsilon_0(15K)$ . The insert shows a magnification of the low driving force region.

To summarize, in this work we reproduced the inverse melting of the vortex matter from BrG phase into the VG phase using numerical simulations and we discussed some of the features characterizing each phase based on quantities measured in the simulations.

*Acknowledgments* - This work is supported by the US Department of Energy (DOE), Grant No. DE-FG02-98ER45686. We also thank the DOE NERSC program and the Pittsburgh Supercomputing Center for time allocations.

- 
- [1] B. Khaykovich *et al.*, Phys. Rev. Lett. **76**, 2555 (1996).
  - [2] B. Khaykovich *et al.*, Phys. Rev. B **56**, R517 (1997).
  - [3] D. T. Fuchs *et al.*, Phys. Rev. Lett. **80**, 4971 (1998).
  - [4] N. Avraham *et al.*, Nature (London) **411**, 451 (2001).
  - [5] H. Beidenkopf *et al.*, Phys. Rev. Lett. **95**, 257004 (2005).
  - [6] H. Beidenkopf *et al.*, Phys. Rev. Lett. **98**, 167004 (2007).
  - [7] T. Giamarchi and P. Le Doussal, Phys. Rev. Lett. **72**, 1530 (1994).
  - [8] D. Ertas and D. Nelson, Physica C **272**, 79 (1996).
  - [9] Y. Y. Goldschmidt, Phys. Rev. B **56**, 2800 (1997).
  - [10] J. Kierfeld and V. Vinokur, Phys. Rev. B **61**, R14928 (2000).
  - [11] D. Li *et al.*, J. Supercond. Nov. Magn., **19**, 369 (2006)
  - [12] S. Ryu *et al.*, Phys. Rev. Lett. **77**, 2300 (1996).
  - [13] A. van Otterlo *et al.*, Phys. Rev. Lett. **81**, 1497 (1998).
  - [14] Y. Nonomura and X. Hu, Phys. Rev. Lett. **86**, 5140 (2001).
  - [15] P. Olsson and S. Teitel Phys. Rev. Lett. **87**, 137001 (2001).
  - [16] C. J. Olson *et al.*, Physica C **384**, 143 (2003).
  - [17] C. Dasgupta and O. T. Valls, Phys. Rev. B **74**, 184513 (2006); *ibid.* **76**, 184509 (2007).
  - [18] J. R. Clem, Phys. Rev. B **43**, 7837 (1991); J. Supercond. **17**, 613 (2004).
  - [19] Y. Y. Goldschmidt, Phys. Rev. B **72**, 064518 (2005)

- [20] Y. Y. Goldschmidt and E. Cuansing, Phys. Rev. Lett. 95, 177004 (2005).
- [21] Y. Y. Goldschmidt and J-T. Liu, Phys. Rev. B **76**, 174508 (2007)
- [22] G. Blatter *et. al.*, Rev. Mod. Phys **66**, 1125 (1994).